Article

On-Demand Degradable and Acid-Generating Polymers Using Phenacyl Ester Derivatives

Hyemi Yeon, Ameet Kumar, Juhwan Song, Juho Lee, Se Jun Wang, Sang Yup Kim, Jinhan Cho, Daeheum Cho,* and Tae Ann Kim*

Read Online

ACCESS | Metrics & More | Article Recommendations | Supporting Information

ABSTRACT: UV-triggered degradation is an efficient method for disposing of polymers that are no longer usable or needed. Although various photolabile molecules have been employed to design photodegradable polymers, the potential of phenacyl ester derivatives, which liberate acidic molecules upon UV exposure, remains largely unexplored in polymer materials. Our study presents the UV-triggered degradation of polymers by utilizing phenacyl ester derivatives as monomers and cross-linkers. Through computational simulations and experiments, we investigate the regioisomeric and substitution effects of these derivatives on UV degradation kinetics. Notably, when incorporating these derivatives as repeating units in linear polymers, we observe accelerated UV degradation kinetics compared with small molecules. Throughout the degradation process, the photogenerated acids effectively initiate the deprotection of acetal protecting groups and the depolymerization of acid-sensitive polymers. Furthermore, we develop UV-degradable thermosetting resins based on phenacyl ester cross-linkers, serving as matrix materials for carbon fiber-reinforced polymer (CFRP) composites. By utilization of the UV-triggered degradation of the resin, CFs can be efficiently retrieved and recycled, offering a sustainable solution for CF recycling. This study opens a new avenue for designing waste-free plastics that can trigger specific chemical reactions upon degradation, contributing to a more environmentally friendly disposal of polymer waste.
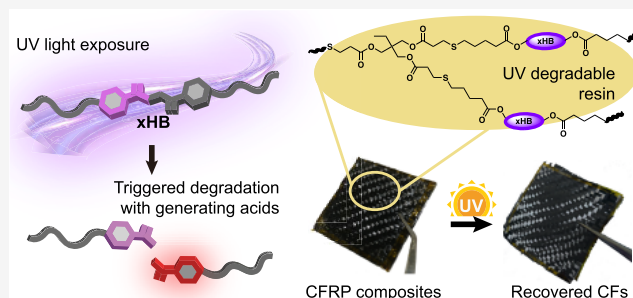
1. INTRODUCTION

A polymer, commonly referred to as a plastic, has been used in nearly every aspect of our daily lives because of its lightweight, versatile mechanical properties, good processability, and excellent stability. However, approximately 50% of plastics are used for single-use disposable applications, such as packaging, agricultural films, and disposable consumer products. After use, most of them are either discarded in landfills or incinerated; only less than 10% have been recycled.[1,2] Unfortunately, physically recycled plastics such as melt-processed and remolded plastics typically have inferior mechanical and thermal properties compared to virgin plastics. Repetitive recycling eventually degrades the performance of the plastics and leads to their end of life.[3] Therefore, one of the desirable final life-cycle steps for the materials is on-demand degradation,[4,5] which is actively triggered by a specific stimulus when they are no longer usable or need to be discarded.

A variety of stimuli have been used to induce on-demand degradation of polymers, including pH, temperature, electrical and magnetic fields, chemical gradients, and light.[6] Light has several unique advantages over other stimuli: (i) accurate control over when and where light irradiates a target area, (ii) easy tuning of stimuli strength by a power and irradiation time, and (iii) applications in noncontact and remote environments.

Despite its diverse advantages, only limited photocleavable functional groups have been incorporated into polymer chains.[7−9] Nitrobenzyl derivatives are among the most popular photolabile moieties in polymer science, especially for in vivo applications because of their biocompatibility after degradation.[10−12] Phenacyl ester derivatives are one of the promising alternatives to the nitrobenzyl groups.[13,14] The major byproduct, hydroxyphenylacetic acid, is water-soluble and nontoxic. The liberated acid upon photochemical activation can be utilized as a catalyst to initiate or regulate an additional reaction. Furthermore, the byproduct shows a hypsochromic shift of UV absorption range compared to the parent molecule so that it does not interfere with light absorption of the parent one. Although phenacyl moieties have been successfully used as protecting groups in organic chemistry, they are rarely used in polymer materials.[15,16]
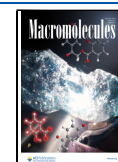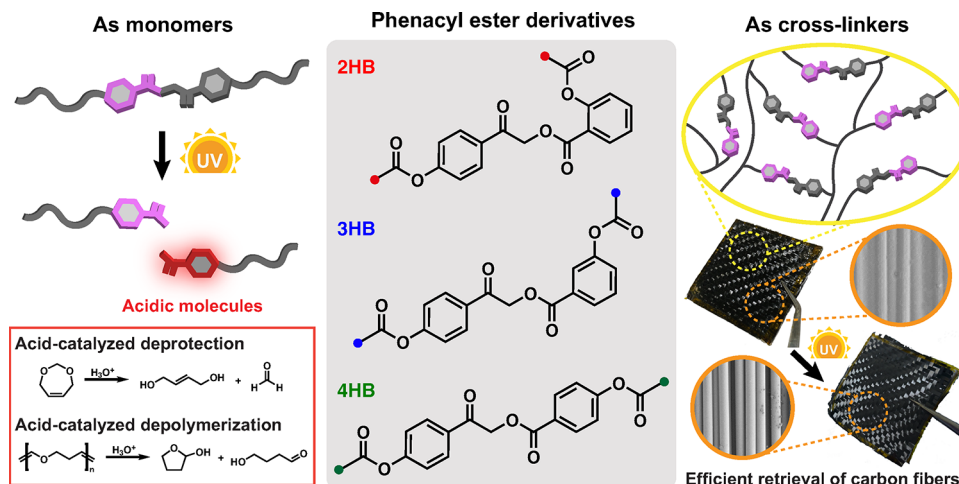
Scheme 1. Phenacyl Ester Derivatives as Multifunctional Photolabile Monomers and Cross-Linkers

UV-triggered degradation of a polymer can be controlled depending on the amount and location of the photocleavable molecules within the polymer structure. When the photocleavable molecules are incorporated as a repeating unit, the polymer network is completely degraded into lower-molecular-weight organic substances or oligomeric units. Additionally, the structure of photoresponsive molecules influences the reactivity of UV degradation. As an example, phenacyl analogues with aryl substitution at the C_α position exhibited different photodegradation efficiency depending on the number and location of the methoxy substituent.[17] Other factors, including the electronic structure, also affect the quantum yield. Substituting electron withdrawing groups such as $-CF_3$ and $-CN$ on the *meta* position of a phenacyl ring enhanced the quantum yield while electron-donating groups such as $-OCH_3$ decreased it.[18]

Herein, we report UV-triggered degradation of thermoplastic and thermosetting polymers using phenacyl ester derivatives as monomers and cross-linkers (Scheme 1). Three regioisomeric phenacyl esters are synthesized and their degradation kinetics under UV light are investigated. Then, we incorporate each phenacyl ester isomer as a repeating unit for linear polymers and compare the degradation kinetics of the polymers with that of small molecules. Computational simulations are performed to elucidate the photodissociation mechanism of phenacyl ester derivatives. Finally, UV-degradable thermosetting resins are prepared to serve as matrix materials for carbon fiber-reinforced polymer (CFRP) composites, allowing nondestructive and effective recovery of expensive CFs simply by exposing UV light.

2. RESULTS AND DISCUSSION

2.1. Phenacyl Ester Regioisomers (xHB). We synthesized three types of phenacyl ester regioisomers (**2HB**, **3HB**, and **4HB**) via a base-catalyzed S_N2 reaction between 2-bromo-4-hydroxyacetophenone and *o*-, *m*-, or *p*-hydroxyphenylacetic acid (Scheme S1). Each isomer has the maximum absorption at around 295 nm, and the molar extinction coefficient (ε) ranges between 7200 and 7800 L mol^{-1} cm^{-1} (Figure S1). ^{1}H NMR spectroscopy was employed to monitor the degradation kinetics of each isomer under a UV lamp fitted with a 312 nm filter (4.3 mW/cm^2, Figure S2) in a hydrogen donor solvent (isopropanol, IPA). UV-stable 3,5-bis(trifluoromethyl)benzoic acid served as an internal standard. During the UV degradation of phenacyl ester derivatives, the α-carbons of both the ketone and ester groups broke down into acetophenone and phenylacetic acid

(Figure 1a). The signal of the α-carbon methylene groups (5.6 ppm, red star in Figures S3 and S5) decreased over time compared to the fixed internal standard concentration (8.4 ppm, blue circle in Figures S3−S5). By assuming first-order reaction kinetics,[19] the change in log concentration of the reactant was plotted against time, and the slope represents the degradation rate constant (k) for each molecule (Figure 1b). **2HB** had the highest k for 7.18 (± 2.33) $\times 10^{-3}$ min^{-1}, while **3HB** exhibited the lowest value for 9.33 (± 5.89) $\times 10^{-4}$ min^{-1}. **4HB** had an intermediate k of 3.01 (± 0.87) $\times 10^{-3}$ min^{-1} between **2HB** and **3HB** (Figure 1c). The effect of IPA concentration on k among the isomers was not apparent (Figure S6). According to the Eyring−Polanyi equation, the rate constant is dependent on the activation energy (ΔE_a), expressed as

$$k = \frac{k_b T}{\hbar} \exp\left(-\frac{\Delta E_a}{k_b T}\right) \tag{1}$$

Here, k_b represents the Boltzmann constant, $\hbar$ is Planck's constant, and T denotes temperature. The activation energies for the UV degradation reactions of **xHB**s were calculated using eq 1,[20] resulting in values of 24.2 ± 0.9 kcal mol^{-1} (**2HB**), 25.9 ± 0.4 kcal mol^{-1} (**3HB**), and 25.2 ± 0.2 kcal mol^{-1} (**4HB**). We also verified that UV degradation of **xHB**s generates acidic substances by noting the color change upon addition of rhodamine B solution (Figure S7).

The relaxed potential energy surface (PES) of **2HB**, **3HB**, and **4HB** with respect to the C1−O2 bond distance in S$_1$, T$_1$, and D$_1$ have been calculated (Figures S8 and 2). In the **xHB** series, the activation barriers for the photodissociation in the S$_1$ and T$_1$ states are higher than that in the D$_1$ state, implying that the photodissociation occurs in the radical state. The photodissociation of the **xHB** series is not likely to occur on the S$_1$ (>32 kcal mol^{-1}) and T$_1$ (>39 kcal mol^{-1}) states due to high activation energies for the photodissociation. The activation energies on the D$_1$ state for **2HB**, **3HB**, and **4HB** were found to be 15.95, 21.21, and 18.45 kcal mol^{-1}, respectively, which can be overcome at room temperature. The results indicate that the rate of the photodissociation of the radicals follows the order of **2HB** > **4HB** > **3HB**, which is consistent with experimental results.

The natural transition orbital (NTO) analysis has been performed at the transition state geometry of S$_1$, T$_1$, and D$_1$ states. The highest occupied natural transition orbital (HONTO) and lowest unoccupied natural transition orbital
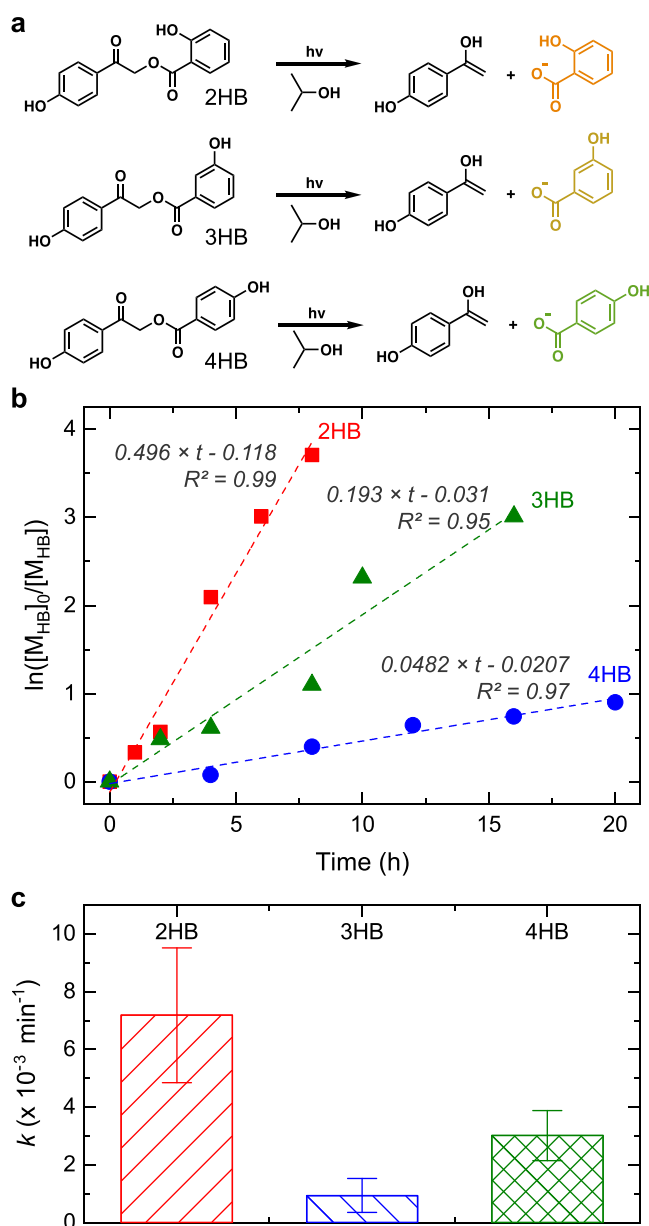
Figure 1. UV degradation of dihydroxy phenacyl ester derivatives. (a) Photocleavage reaction scheme, (b) kinetic plots of reactant concentration vs time, and (c) the average degradation rate constant (k) for **2HB**, **3HB**, and **4HB**. Error bars represent one standard deviation of the data.

(LUNTO) are calculated. The electron transition occurs from the HONTO (hole) to the LUNTO (excited electron). We observed that a charge is transferred from the left benzene ring to the right benzene ring from the NTOs of D_1 at the transition state (Figure 3). The NTO analysis indicated that in LUNTO of the **2HB** in the D_1 state, electron delocalization is observed on the *ortho* hydroxyl (OH) group which stabilizes the D_1 state, resulting in the reduced activation barrier for the photodissociation (faster photodissociation). While in LUNTO of the **3HB** in the D_1 state, no electron delocalization was observed on the OH group due to the substitution at the *meta* position which destabilizes the D_1 state, resulting in a higher barrier than that of the **2HB**. The electron delocalization was observed at the *para* OH group in the LUNTO of **4HB** in the D_1 state, which leads to the lower barrier than the **3HB**. These findings suggest that the

position of the OH substituent and the corresponding electron delocalization patterns play critical roles in the photodissociation of **xHB** compounds.

2.2. Linear Copolymers Composed of Phenacyl Ester Derivatives (P-xHB). We synthesized UV-degradable alternating copolymers by incorporating **xHB** units into the main chain via Pt-catalyzed hydrosilylation.[21,22] Initially, bis-alkene-functionalized **xHBs** (**xHB-pen**) were synthesized (Scheme S2) and polymerized with 1,1,3,3,5,5-hexamethyltrisiloxane using Karstedt's catalyst (Figure 4a). Since the concentration of the monomer influenced the molecular weight of the resulting polymer, the minimum amount of the solvent was used to dissolve the monomer for polymerization. All **HB**-incorporated polymers were adjusted to a molecular weight of approximately 10,000 g mol^{-1}, and further details for each sample are included in the Supporting Information (Figures S9–S11 for NMR spectra and Figure S12 for GPC results).

After each polymer was dissolved in a THF:IPA (4:1 v/v) mixture and irradiated with UV light, the ^{1}H NMR spectra of the samples were monitored at regular intervals to confirm the photocleavage of the phenacyl ester derivatives. The peak of the α-carbon methylene groups (5.6 ppm, red star in Figure S13) in phenacyl esters decreased over time and disappeared within 120 min for all regioisomers unlike dihydroxy phenacyl ester derivatives. When the degradation rate constants for **xHBs** incorporated into polymers were calculated by assuming the first-order reaction kinetics, the values were found to be approximately 0.015 min^{-1}, which is approximately 2 orders of magnitude higher than those of the dihydroxy phenacyl ester derivatives (Figure 4). We did not find any statistically significant difference in the degradation kinetics depending on the regioisomers. To explore the reason for the accelerated UV degradation rate of **P-xHBs**, we measured their molar extinction coefficients (ε) (Figure S14). It is noteworthy that phenacyl ester units in copolymers showed two times higher values of ε compared to dihydroxy phenacyl ester derivatives. We suspect that increased light absorption ability in the polymers would accelerate the UV degradation behaviors of **P-xHBs**.

Due to the degradation of phenacyl esters in the main chain, the molecular weights of **P-xHBs** steadily decreased over time upon UV exposure, and the signal was moved toward undetectable regions within 60 min (Figure S15). To confirm that the degradation of these polymers is triggered by phenacyl ester derivatives, control samples were synthesized by incorporating bisphenol A instead of phenacyl esters. Under the same UV exposure conditions, the control samples did not exhibit any significant changes in chemical structures or molecular weight (Figure S16).

The PES and the NTO analyses of the **xHB-pen** series were performed instead of the **P-xHBs** due to the computational difficulties of calculating the excited-state properties of the polymer in the solid state. We believe that a similar photodissociation mechanism may apply to the **xHB-pen** and **P-xHB** series. The PES analysis shows that the reaction barriers of **2HB-pen**, **3HB-pen**, and **4HB-pen** in S_1 (>37 kcal mol^{-1}) and T_1 (>35 kcal mol^{-1}) states were higher than the D_1 excited state, implying that the photodissociation occurs in the radical form (Figure 5). The reaction barriers in the D_1 state were found to be similar in **2HB-pen** (20.06 kcal mol^{-1}), **3HB-pen** (21.67 kcal mol^{-1}), and **4HB-pen** (18.90 kcal mol^{-1}), which suggests that they have similar photodissociation rates.

The NTO analysis was performed at the transition state for the photodissociation of the **xHB-pen** series in the D_1 state
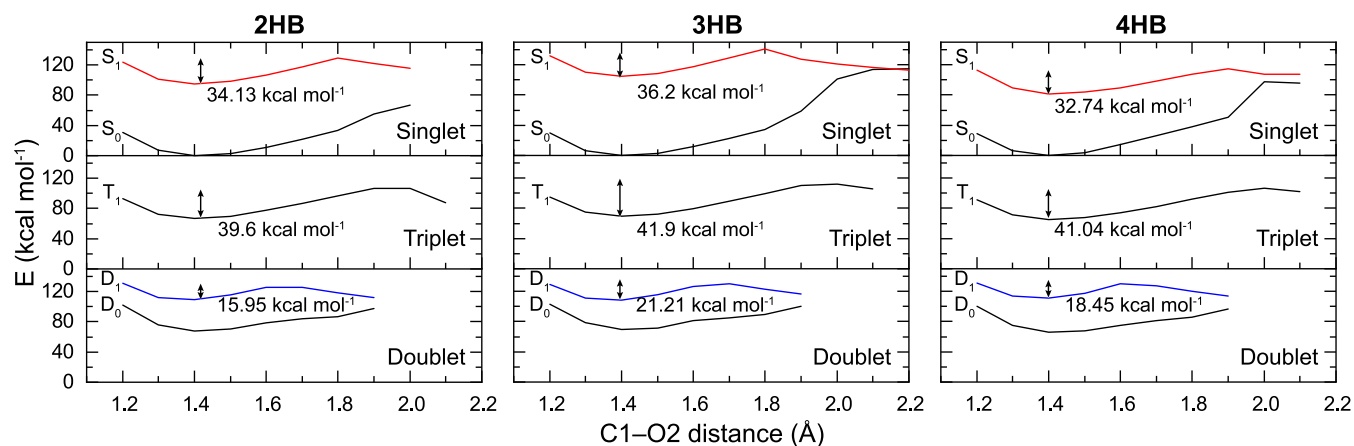
Figure 2. Relaxed potential energy surface of **xHB** in singlet, triplet, and doublet (radical) states. The activation barriers for the photodissociation are marked.
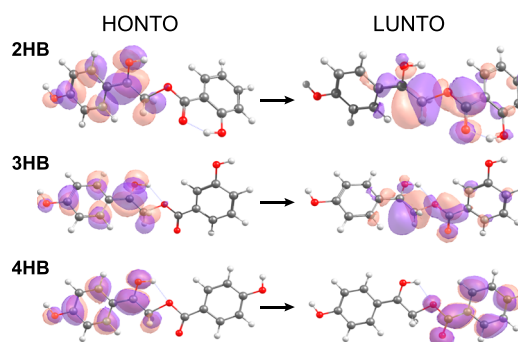
Figure 3. NTO analysis of **2HB**, **3HB**, and **4HB** in the transition state of D_1 at an isovalue of 0.03 e/Å^3.

(Figure 6). In the LUNTOs, the absence of electron delocalization on the ester group regardless of the position of the substituents of the **xHB-pen** series indicates that the **xHB-pen** series have similar photodissociation rates, which is consistent with the experimental findings.

Therefore, we anticipate that the type of substituents on phenacyl ester regioisomers is a crucial factor influencing their photodissociation kinetics. Specifically, with hydroxyl substituents (**xHB**), the electron delocalization pattern undergoes significant alteration depending on the substituent's position, resulting in distinct photodissociation kinetics among the regioisomers. Conversely, for ester substituents (**xHB-pen** and **P-xHB**), electron delocalization is limited, minimizing the regioisomeric effect on photodissociation kinetics.

**2.3. Utilization of Photogenerated Acids from P-2HBs.** The generation of acids from **P-xHB**s after UV exposure was confirmed through a rhodamine B test.[23,24] When the pristine **P-xHB** solution was mixed with a rhodamine B solution, it remained colorless. However, when the UV-treated solutions, which were initially colorless, were mixed with the rhodamine B solution, a vibrant pink color appeared, indicating the protonation of rhodamine B. The generation of acid was further verified by UV–vis absorption spectroscopy, as the spectrum of the UV-treated polymers with the indicator solution matched that of protonated rhodamine B (Figures 7a and S17).

Photogenerated acids can be effectively utilized to initiate various reactions such as functional group deprotection, hydrolysis, and polymerization or depolymerization.[25−29] Initially, we demonstrated the successful deprotection of cyclic
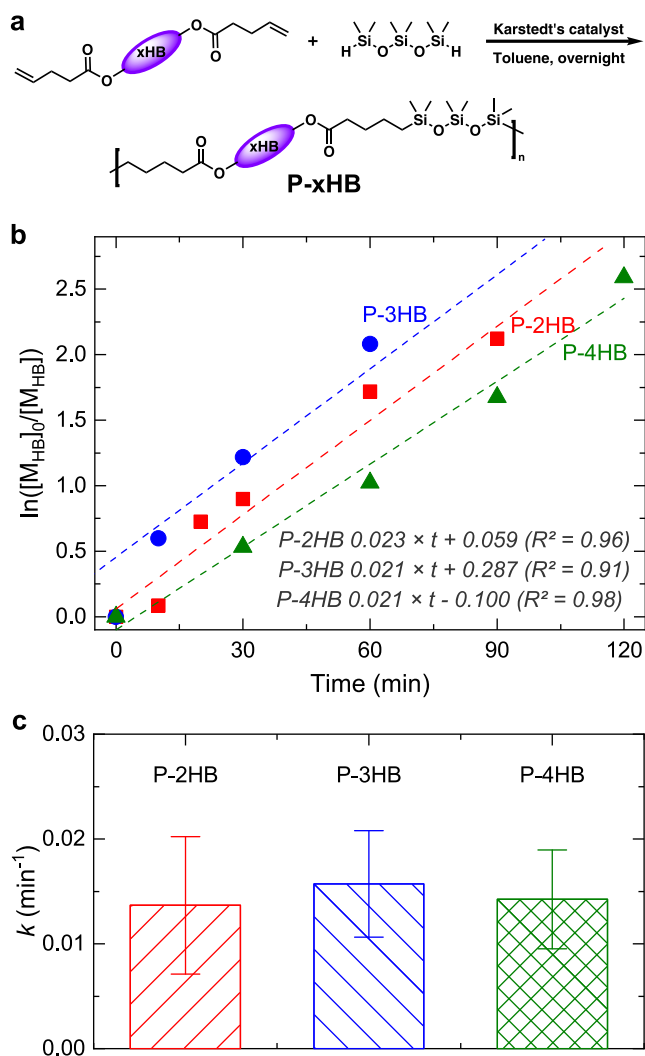

Figure 4. Phenacyl ester incorporated linear polymers (**P-xHB**s) and their UV degradation kinetics. (a) Synthetic scheme of **P-xHB**, (b) kinetic plots of reactant concentration vs time, and (c) the average degradation rate constant (k) for **P-2HB**, **P-3HB**, and **P-4HB**. Error bars represent one standard deviation of the data.

acetals using acids generated from **P-2HB**s.[30] Specifically, 1,3-dioxep-5-ene (0.02 mM) was dissolved in UV-treated **P-2HB**
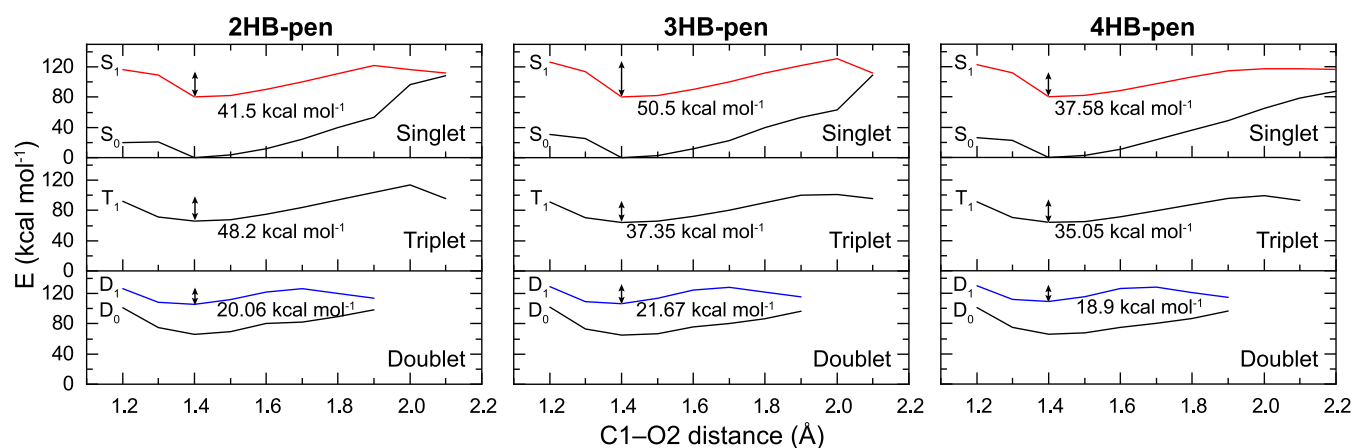
Figure 5. Potential energy surface (PES) analysis of radicals of **2HB-pen**, **3HB-pen**, and **4HB-pen**. The activation barriers for the photodissociation are marked.
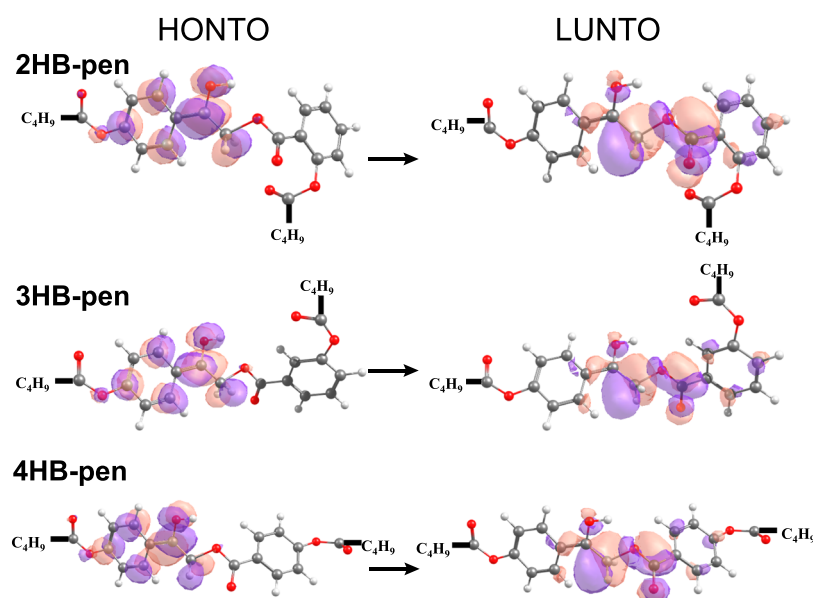

Figure 6. NTO analysis of **2HB-pen**, **3HB-pen**, and **4HB-pen** at the transition state in the D_1 state at an isovalue of 0.03 e/Å^3.
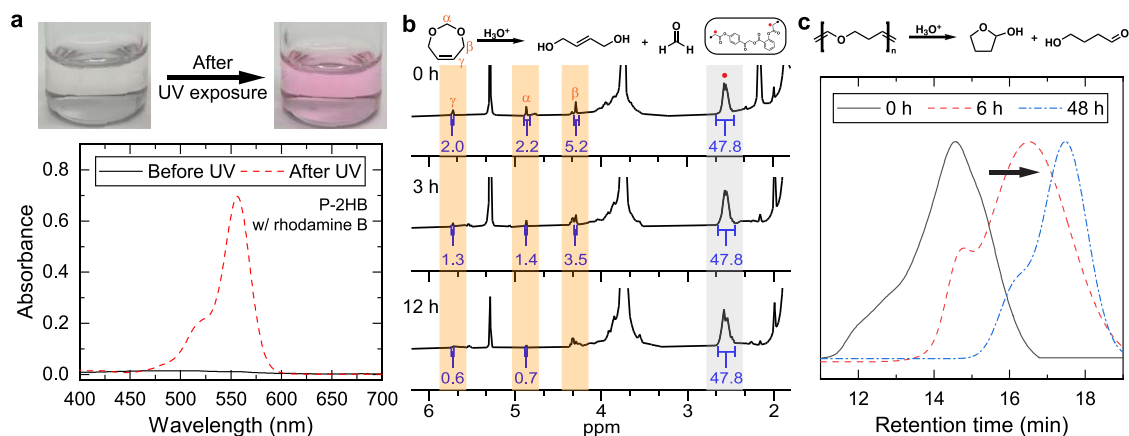
Figure 7. Acid generation from P-2HB. (a) Change in absorbance before and after UV exposure for **P-2HB** in a rhodamine B solution. (b) Acid-catalyzed deprotection of cyclic acetal (1,3-dioxep-5-ene). (c) Degradation of poly(2,3-dihydrofuran) in an acidic environment.

solution, and the change in the NMR spectrum was monitored with time (Figure 7b). As a result of the acid-triggered deprotection reaction, the integral values of characteristic

peaks corresponding to the cyclic acetals (α, β, and γ) gradually decreased relative to the α-hydrogens originating from carbonyl groups of **P-2HB**s (indicated by the red circle). Additionally, we
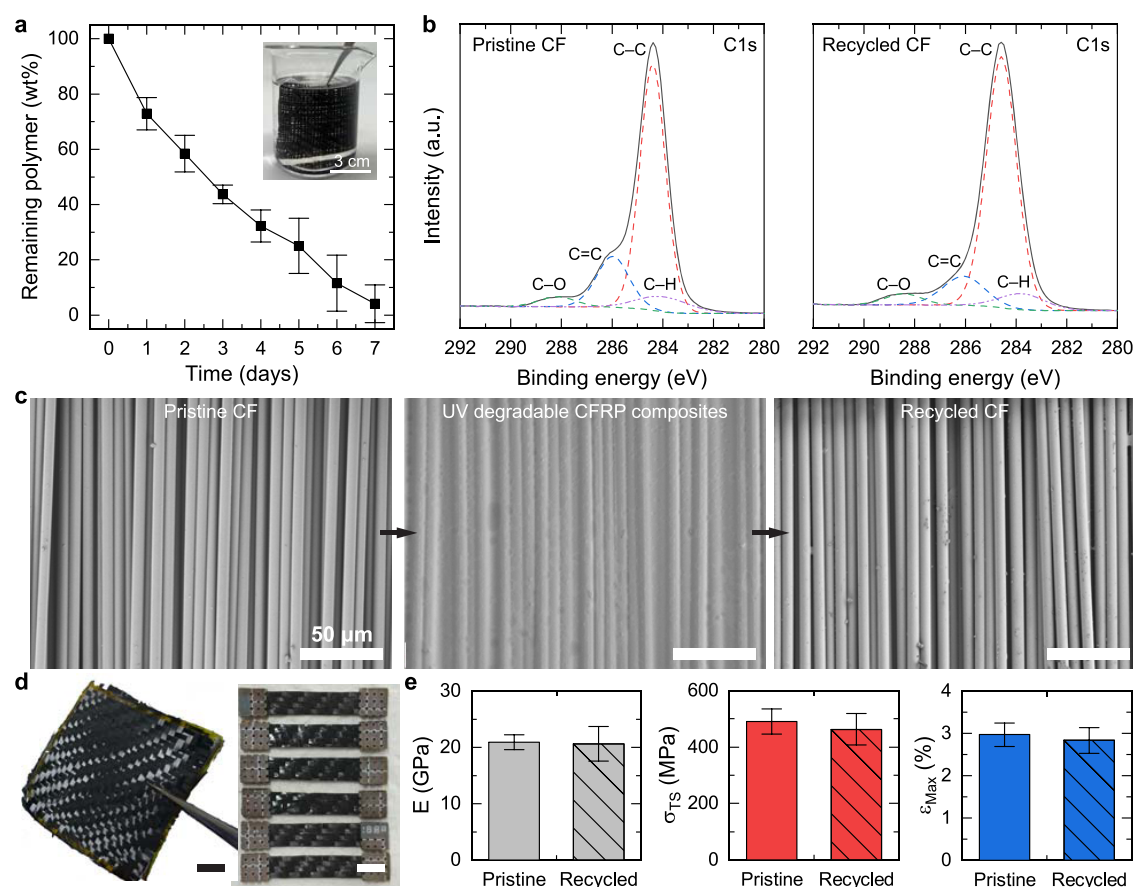
Figure 8. UV degradation of cross-linked resins for CFRP composites and their mechanical properties. (a) Remaining polymer weights of **2HB-pen** incorporated cross-linked polymers in CFRP composites with UV-exposed time. (b) XPS spectra of pristine CF and recycled CF in the C 1s region. (c) SEM images of pristine CF, CFRP composite, and recycled CF. (d) Digital images of recycled CFs and their CFRP composites. (e) Elastic modulus (E), tensile strength (σ_{TS}), and failure strain (ϵ_{max}) for both composites. Reported values and error bars represent the average and one standard deviation, respectively.

employed the photogenerated acids to depolymerize acid-sensitive polymers, poly(2,3-dihydrofuran) (PDHF).[31,32] 10 mg of PDHF (M_n = 45,000 g mol^{-1}) was dissolved in UV-exposed **P-2HB** solution, and the changes in molecular weight of PDHF were measured over time. Within a period of 48 h, the PDHF polymer underwent degradation into smaller molecules. We attribute the relatively slow degradation rate to the moderate strength of the photogenerated acids. Furthermore, the kinetics of acid-triggered reactions can be controlled by adjusting the strength and duration of UV light exposure to **xHB**-incorporated polymers.

2.4. Carbon Fiber-Reinforced Polymer (CFRP) Composites Using Phenacyl Ester Derivatives. Due to the high production cost of CFs, it is highly desirable to recover and recycle CFs from discarded CFRPs without compromising their integrity.[33−37] One approach is to utilize degradable thermosets that can depolymerize under specific conditions, offering an efficient recycling solution for CFs.[38−43] We synthesized UV-degradable cross-linked polymers through a thiol−ene reaction between bis-alkene-functionalized phenacyl ester derivatives (**2HB-pen**) and trimethylolpropane tris(3-mercaptopropionate)[44−47] and incorporated these polymers as the matrix of CFRP composites (Scheme S3).

The degradation rates of the cross-linked polymers as the matrix of CFRPs were assessed by measuring their relative weights after UV exposure. Pristine CFs and the CFRP composites were immersed in a quartz beaker filled with a THF/IPA (9:1 v/v) mixture. While the pristine CF mats did not exhibit a significant mass change over time (Figure S18), the CFRP composites showed that approximately 50% of the matrix was degraded within 2 days, with complete removal achieved after 7 days (Figure 8a). The slower degradation kinetics of the cross-linked polymers compared to linear polymers can be attributed to the inefficient UV absorption by the UV-absorbing CFs. XPS measurements were conducted to study the surface properties of the recovered CFs and the pristine CFs (Figure 8b).[48−50] The peak patterns and chemical bond percentages of the recovered CFs closely resembled those of the pristine CFs, indicating the successful recovery of the CFs without significant structural changes. Furthermore, SEM analysis was conducted to examine the microstructures of pristine CFs, CFRP composites, and recycled CFs (Figure 8c). The recycled CFs exhibited a clean and smooth surface without noticeable cracks and defects, showing no visible difference from pristine CFs. These XPS and SEM data suggest that the cross-linked polymers were completely removed by UV exposure and the CFs were effectively retrieved from the thermosetting CFRP composites. While our study primarily focuses on photochemical reactions in solution, it is important to consider how these findings apply to solvent-free conditions for practical polymer waste disposal. Further research should be required to correlate the solution phase with solid-state efficiencies in photochemical reactions.

Using recycled CFs, we refabricated CFRP composites and investigated their quasi-static tensile properties to evaluate the CFRP composites prepared from fresh CFs and recycled CFs (Figures 8d and S19). Both CFRP composites exhibited brittle failure without a yield point and maintained the same level of the elastic modulus (20.1 ± 1.3 GPa vs 20.6 ± 3.1 GPa), ultimate strength (490.3 ± 44.3 MPa vs 463.2 ± 55.7 MPa), and failure strain ($2.96 \pm 0.27\%$ vs $2.84 \pm 0.30\%$) (Figure 8e). Since the ultimate strength of the CFRP composite is mainly determined by the CFs,[51,52] the consistency in the material strength further confirms that the CFs remained intact throughout the UV degradation process.

3. CONCLUSIONS

We have successfully demonstrated phenacyl ester derivatives as UV-degradable monomers and cross-linkers for UV-transient thermoplastic or thermosetting polymers. We initially investigated the UV degradation kinetics of the dihydroxy-terminated phenacyl ester regioisomers (**xHB**s) and found that the position of the hydroxyl group significantly influenced their degradation rate constants. When each regioisomer (**xHB-pen**) was incorporated into linear copolymers (**P-xHB**), we observed no statistical difference in the UV degradation rates. DFT results further supported the regioisomeric and substitution effects of phenacyl ester derivatives on their UV degradation kinetics. Additionally, we utilized the acid byproducts generated from photodissociation of phenacyl esters for the deprotection of acetals and the degradation of acid-sensitive polymers. Finally, we incorporated one of phenacyl ester derivatives into thermosetting CFRP resins and confirmed the efficient retrieval of precious CFs without any physical or chemical damage. We envision that these phenacyl ester derivatives hold promising potential for designing on-demand degradable polymers in various fields including packaging, electronics, and drug delivery systems.

4. EXPERIMENTAL SECTION

4.1. Materials. Unless otherwise stated, all reagents were purchased from commercial source and used as received. Azobis(isobutyronitrile) (AIBN) (98%) was recrystallized before use.

4.2. Synthesis of HB-Incorporated Alternating Copolymers (P-xHB). A two-neck round-bottom flask equipped with a condenser and N_2 inlet adapter was charged with **xHB-pen** (0.33 g, 0.75 mmol, 1.0 equiv), 1,1,3,3,5,5-hexamethyltrisiloxane (0.16 g, 0.75 mmol, 1.0 equiv), and anhydrous toluene. Then, platinum 1,3-divinyltetramethyldisiloxane complex (in xylene, ~2% Pt) was added. The reaction mixture was heated at 80 °C and stirred overnight. The resulting viscous solution was precipitated in methanol and washed several times. The precipitate was dried in a vacuum oven for 24 h at 60 °C.

4.3. Fabrication of HB-Incorporated CFRP Composites. The cross-linked polymers were synthesized by using the following procedures. Initially, **2HB-pen** (0.51 g, 1.17 mmol, 1.0 equiv) and trimethylolpropane tris(3-mercaptopropionate) (0.31 g, 0.78 mmol, 0.67 equiv) were dissolved in 1 mL of dimethylformamide. An AIBN initiator (5 wt %) was added to the mixture and stirred using a vortex mixer. CF woven fabrics (HexTow AS4C, 3k twill) were cut into 55×55 mm^2 pieces, and two layers of them were placed in the mold. The reaction mixture was evenly applied to the CF fabrics by a wet hand lay-up process, and the composite panel is consolidated after being dried in a vacuum oven, followed by curing at 80 °C for 24 h.

4.4. Computational Details. Density functional theory (DFT) and time-dependent DFT (TD-DFT) calculations were performed to investigate the photodissociation mechanism of the **xHB** and **xHB-pen** series. The PES of the S_1, T_1, and D_1 states along the C1−O2 bond distance were calculated at the CAM-B3LYP/cc-pVDZ level of

theory.[53] The NTO analysis was performed to identify the electronic structure at the transition states for the photodissociation. All of the calculations were carried out by using the ORCA 5.0.3 program.[54]

4.5. Characterization. ^{1}H NMR and ^{13}C NMR spectra were measured on a Bruker Avance III 400 MHz NMR spectrometer. Spectra were referenced to the residual solvent peak: chloroform-d (^{1}H NMR: 7.24 ppm, ^{13}C NMR: 77.23 ppm) or dimethyl sulfoxide-d_6 (^{1}H NMR: 2.50 ppm, ^{13}C NMR: 39.52 ppm). Gel permeation chromatography (GPC) measurements were carried out on an Agilent 1260 Infinity II equipped with a 1260 Infinity II refractive index detector (RID) and two PLgel 10 mm MIXED-B columns with a prefilter. Tetrahydrofuran (inhibitor free, HPLC grade, Tedia) was used as an eluent with a flow rate of 1 mL/min. The molecular weights were calibrated by using uniform polystyrene standards. The UV−vis absorption spectra were recorded by using a Jasco V-670 spectrophotometer. The surface morphologies of CF and CFRP were observed with scanning electron microscopy (SEM) (Sigma 300, ZEISS). The composition of elements on the sample surface was characterized by using X-ray photoelectron spectroscopy (XPS) (K-Alpha+, Thermo Fisher Scientific). Thermogravimetric analysis (TGA) (Q50, TA Instruments) was performed to determine the residual mass of the resin in the CFs. The temperature was increased by 10 °C min^{-1} to 700 °C, and the nitrogen flow rate was 100 cm^3 min^{-1}. A universal testing machine (UTM, 5567, Instron) was used to test the tensile strength. Here, all of the fiber fabrics were cut into the same dimension (115.6 mm in length and 22.3 mm in width) with 11 bundles along the stretching direction. Since the fiber fabrics are plain woven fabrics, we anticipate a minimum influence on the uniaxial tension behavior from the fiber bundles oriented perpendicular to the stretching direction. At least five samples were tested at a constant displacement rate (1 mm min^{-1}).

■ ASSOCIATED CONTENT

Ⓢ **Supporting Information**

The Supporting Information is available free of charge at https://pubs.acs.org/doi/10.1021/acs.macromol.3c02136.

> Synthesis and characterization of **xHB**, **xHB**-incorporated copolymers, control samples, simulation models, synthetic scheme for cross-linked polymers, tensile properties of pristine and recycled CFRPs, and NMR spectra of small molecules (PDF)

■ AUTHOR INFORMATION

Corresponding Authors

Daeheum Cho − *Department of Chemistry, Kyungpook National University, Daegu 41566, Republic of Korea;* Ⓞ orcid.org/0000-0002-0322-4291; Email: daeheumc@knu.ac.kr

Tae Ann Kim − *Solutions to Electromagnetic Interference in Future-mobility Research Center, Korea Institute of Science and Technology, Seoul 02792, Republic of Korea; Soft Hybrid Materials Research Center, Korea Institute of Science and Technology, Seoul 02792, Republic of Korea; Division of Energy & Environment Technology, KIST School, Korea University of Science and Technology (UST), Seoul 02792, Republic of Korea;* Ⓞ orcid.org/0000-0002-1084-638X; Email: takim717@kist.re.kr

Authors

Hyemi Yeon − *Solutions to Electromagnetic Interference in Future-mobility Research Center, Korea Institute of Science and Technology, Seoul 02792, Republic of Korea; Department of Chemical and Biological Engineering, Korea University, Seoul 02841, Republic of Korea*

Ameet Kumar − *Department of Chemistry, Kyungpook National University, Daegu 41566, Republic of Korea*

Juhwan Song − *Solutions to Electromagnetic Interference in Future-mobility Research Center, Korea Institute of Science and Technology, Seoul 02792, Republic of Korea*

Juho Lee − *Solutions to Electromagnetic Interference in Future-mobility Research Center, Korea Institute of Science and Technology, Seoul 02792, Republic of Korea*

Se Jun Wang − *Department of Mechanical Engineering, Sogang University, Seoul 04107, Republic of Korea*

Sang Yup Kim − *Department of Mechanical Engineering, Sogang University, Seoul 04107, Republic of Korea*

Jinhan Cho − *Department of Chemical and Biological Engineering, Korea University, Seoul 02841, Republic of Korea;* ⊙ orcid.org/0000-0002-7097-5968

Complete contact information is available at:
https://pubs.acs.org/10.1021/acs.macromol.3c02136

Notes

The authors declare no competing financial interest.

■ ACKNOWLEDGMENTS

■ REFERENCES

(1) Geyer, R.; Jambeck, J. R.; Law, K. L. Production, Use, and Fate of All Plastics Ever Made. *Sci. Adv.* **2017**, *3* (7), No. e1700782.

(2) Rahimi, A.; García, J. M. Chemical Recycling of Waste Plastics for New Materials Production. *Nat. Rev. Chem.* **2017**, *1* (6), No. 0046.

(3) Feng, H.; Xu, X.; Wang, B.; Su, Y.; Liu, Y.; Zhang, C.; Zhu, J.; Ma, S. Facile Preparation, Closed-Loop Recycling of Multifunctional Carbon Fiber Reinforced Polymer Composites. *Composites, Part B* **2023**, *257*, No. 110677.

(4) Patrick, J. F.; Robb, M. J.; Sottos, N. R.; Moore, J. S.; White, S. R. Polymers with Autonomous Life-Cycle Control. *Nature* **2016**, *540* (7633), 363−370.

(5) Utekar, S.; V K, S.; More, N.; Rao, A. Comprehensive Study of Recycling of Thermosetting Polymer Composites − Driving Force, Challenges and Methods. *Composites, Part B* **2021**, *207*, No. 108596.

(6) Kamaly, N.; Yameen, B.; Wu, J.; Farokhzad, O. C. Degradable Controlled-Release Polymers and Polymeric Nanoparticles: Mechanisms of Controlling Drug Release. *Chem. Rev.* **2016**, *116* (4), 2602−2663.

(7) Pasparakis, G.; Manouras, T.; Argitis, P.; Vamvakaki, M. Photodegradable Polymers for Biotechnological Applications. *Macromol. Rapid Commun.* **2012**, *33* (3), 183−198.

(8) Huang, Q.; Bao, C.; Ji, W.; Wang, Q.; Zhu, L. Photocleavable Coumarin Crosslinkers Based Polystyrene Microgels: Phototriggered Swelling and Release. *J. Mater. Chem.* **2012**, *22* (35), 18275−18282.

(9) Xiao, P.; Zhang, J.; Zhao, J.; Stenzel, M. H. Light-Induced Release of Molecules from Polymers. *Prog. Polym. Sci.* **2017**, *74*, 1−33.

(10) Thomas, S. W. New Applications of Photolabile Nitrobenzyl Groups in Polymers. *Macromol. Chem. Phys.* **2012**, *213* (23), 2443−2449.

(11) Ahmad, M.; Roy, N. J.; Singh, A.; Mondal, D.; Mondal, A.; Vijayakanth, T.; Lahiri, M.; Talukdar, P. Photocontrolled Activation of Doubly O-Nitrobenzyl-Protected Small Molecule Benzimidazoles Leads to Cancer Cell Death. *Chem. Sci.* **2023**, *14* (33), 8897−8904.

(12) Milani, A. H.; Saunders, J. M.; Nguyen, N. T.; Wu, S.; Saunders, B. R. Light-Triggered Programming of Hydrogel Properties Using Sleeping Photoactive Polymer Nanoparticles. *Chem. Mater.* **2021**, *33* (7), 2319−2330.

(13) Pellicciioli, A. P.; Wirz, J. Photoremovable Protecting Groups: Reaction Mechanisms and Applications. *Photochem. Photobiol. Sci.* **2002**, *1* (7), 441−458.

(14) Bochet, C. G. Photolabile Protecting Groups and Linkers. *J. Chem. Soc. Perkin 1* **2002**, *2* (2), 125−142.

(15) Bertrand, O.; Gohy, J. F.; Fustin, C. A. Synthesis of Diblock Copolymers Bearing p -Methoxyphenacyl Side Groups. *Polym. Chem.* **2011**, *2* (10), 2284−2292.

(16) Sun, S.; Chamsaz, E. A.; Joy, A. Photoinduced Polymer Chain Scission of Alkoxyphenacyl Based Polycarbonates. *ACS Macro Lett.* **2012**, *1* (10), 1184−1188.

(17) Sheehan, J. C.; Wilson, R. M.; Oxford, A. W. Photolysis of Methoxy-Substituted Benzoin Esters. Photosensitive Protecting Group for Carboxylic Acids. *J. Am. Chem. Soc.* **1971**, *93* (26), 7222−7228.

(18) Klán, P.; Šolomek, T.; Bochet, C. G.; Blanc, A.; Givens, R.; Rubina, M.; Popik, V.; Kostikov, A.; Wirz, J. Photoremovable Protecting Groups in Chemistry and Biology: Reaction Mechanisms and Efficacy. *Chem. Rev.* **2013**, *113* (1), 119−191.

(19) Literák, J.; Dostálová, A.; Klán, P. Chain Mechanism in the Photocleavage of Phenacyl and Pyridacyl Esters in the Presence of Hydrogen Donors. *J. Org. Chem.* **2006**, *71* (2), 713−723.

(20) Kim, T. A.; Beiermann, B. A.; White, S. R.; Sottos, N. R. Effect of Mechanical Stress on Spiropyran-Merocyanine Reaction Kinetics in a Thermoplastic Polymer. *ACS Macro Lett.* **2016**, *5* (12), 1312−1316.

(21) Naganawa, Y.; Inomata, K.; Sato, K.; Nakajima, Y. Hydrosilylation Reactions of Functionalized Alkenes. *Tetrahedron Lett.* **2020**, *61* (11), No. 151513.

(22) Grunlan, M. A.; Mabry, J. M.; Weber, W. P. Synthesis of Fluorinated Copoly(Carbosiloxane)s by Pt-Catalyzed Hydrosilylation Copolymerization. *Polymer* **2003**, *44* (4), 981−987.

(23) Diesendruck, C. E.; Steinberg, B. D.; Sugai, N.; Silberstein, M. N.; Sottos, N. R.; White, S. R.; Braun, P. V.; Moore, J. S. Proton-Coupled Mechanochemical Transduction: A Mechanogenerated Acid. *J. Am. Chem. Soc.* **2012**, *134* (30), 12446−12449.

(24) Lin, Y.; Kouznetsova, T. B.; Craig, S. L. A Latent Mechanoacid for Time-Stamped Mechanochromism and Chemical Signaling in Polymeric Materials. *J. Am. Chem. Soc.* **2020**, *142* (1), 99−103.

(25) Frenette, M.; Coenjarts, C.; Scaiano, J. C. Mapping Acid-Catalyzed Deprotection in Thin Polymer Films: Fluorescence Imaging Using Prefluorescent 7-Hydroxycoumarin Probes. *Macromol. Rapid Commun.* **2004**, *25* (18), 1628−1631.

(26) Teng, C. J.; Weber, W. P.; Cai, G. Acid and Base Catalyzed Ring-Opening Polymerization of 2,2,4,4,6,6-Hexamethyl-8,8-Diphenylcyclotetrasiloxane. *Polymer* **2003**, *44* (15), 4149−4155.

(27) Delcroix, D.; Martín-Vaca, B.; Bourissou, D.; Navarro, C. Ring-Opening Polymerization of Trimethylene Carbonate Catalyzed by Methanesulfonic Acid: Activated Monomer versus Active Chain End Mechanisms. *Macromolecules* **2010**, *43* (21), 8828−8835.

(28) Tsao, C. T.; Chang, C. H.; Lin, Y. Y.; Wu, M. F.; Han, J. L.; Hsieh, K. H. Kinetic Study of Acid Depolymerization of Chitosan and Effects of Low Molecular Weight Chitosan on Erythrocyte Rouleaux Formation. *Carbohydr. Res.* **2011**, *346* (1), 94−102.

(29) Rahimi, A.; Ulbrich, A.; Coon, J. J.; Stahl, S. S. Formic-Acid-Induced Depolymerization of Oxidized Lignin to Aromatics. *Nature* **2014**, *515* (7526), 249−252.

(30) Jarowicki, K.; Kocienski, P. Protecting Groups. *J. Chem. Soc. Perkin 1* **2000**, No. 16, 2495−2527.

(31) Feist, J. D.; Xia, Y. Enol Ethers Are Effective Monomers for Ring-Opening Metathesis Polymerization: Synthesis of Degradable and Depolymerizable Poly(2,3-Dihydrofuran). *J. Am. Chem. Soc.* **2020**, *142* (3), 1186−1189.

(32) Feist, J. D.; Lee, D. C.; Xia, Y. A Versatile Approach for the Synthesis of Degradable Polymers via Controlled Ring-Opening Metathesis Copolymerization. *Nat. Chem.* **2022**, *14* (1), 53−58.

(33) Yu, K.; Shi, Q.; Dunn, M. L.; Wang, T.; Qi, H. J. Carbon Fiber Reinforced Thermoset Composite with Near 100% Recyclability. *Adv. Funct Mater.* **2016**, *26* (33), 6098−6106.

(34) Yao, S. S.; Jin, F. L.; Rhee, K. Y.; Hui, D.; Park, S. J. Recent Advances in Carbon-Fiber-Reinforced Thermoplastic Composites: A Review. *Composites, Part B* **2018**, *142*, 241−250.

(35) Zhang, J.; Chevali, V. S.; Wang, H.; Wang, C. H. Current Status of Carbon Fibre and Carbon Fibre Composites Recycling. *Composites, Part B* **2020**, *193*, No. 108053.

(36) You, J.; Lee, Y. M.; Choi, H. H.; Kim, T. A.; Lee, S. S.; Park, J. H. Thermally Stable and Highly Recyclable Carbon Fiber-Reinforced Polyketone Composites Based on Mechanochemical Bond Formation. *Composites, Part A* **2021**, *142* (December 2020), No. 106251.

(37) Lloyd, E. M.; Lopez Hernandez, H.; Feinberg, A. M.; Yourdkhani, M.; Zen, E. K.; Mejia, E. B.; Sottos, N. R.; Moore, J. S.; White, S. R. Fully Recyclable Metastable Polymers and Composites. *Chem. Mater.* **2019**, *31* (2), 398−406.

(38) Wang, B.; Ma, S.; Yan, S.; Zhu, J. Readily Recyclable Carbon Fiber Reinforced Composites Based on Degradable Thermosets: A Review. *Green Chem.* **2019**, *21* (21), 5781−5796.

(39) Qiao, Z.; Wang, M.; Jiang, J.; Liu, H.; Wang, M.; Zhao, W.; Wang, Z. High-Performance and Degradable Polybenzoxazine/VU Vitrimer and Its Application for Carbon Fiber Recycling. *ACS Sustainable Chem. Eng.* **2022**, *10* (28), 9113−9122.

(40) Ma, S.; Webster, D. C. Degradable Thermosets Based on Labile Bonds or Linkages: A Review. *Prog. Polym. Sci.* **2018**, *76*, 65−110.

(41) Zieger, M. M.; Mueller, P.; Quick, A. S.; Wegener, M.; Barner-Kowollik, C. Cleaving Direct-Laser-Written Microstructures on Demand. *Angew. Chem., Int. Ed.* **2017**, *56* (20), 5625−5629.

(42) Sangermano, M.; Tonin, M.; Yagci, Y. Degradable Epoxy Coatings by Photoinitiated Cationic Copolymerization of Bisepoxide with ε-Caprolactone. *Eur. Polym. J.* **2010**, *46* (2), 254−259.

(43) Wang, S.; Fu, D.; Wang, X.; Pu, W.; Martone, A.; Lu, X.; Lavorgna, M.; Wang, Z.; Amendola, E.; Xia, H. High Performance Dynamic Covalent Crosslinked Polyacylsemicarbazide Composites with Self-Healing and Recycling Capabilities. *J. Mater. Chem. A* **2021**, *9* (7), 4055−4065.

(44) Kade, M. J.; Burke, D. J.; Hawker, C. J. The Power of Thiol-Ene Chemistry. *J. Polym. Sci., Part A: Polym. Chem.* **2010**, *48* (4), 743−750.

(45) Hoyle, C. E.; Bowman, C. N. Thiol−Ene Click Chemistry. *Angew. Chem., Int. Ed.* **2010**, *49* (9), 1540−1573.

(46) Ji, Y.; Wen, Z.; Fan, J.; Zeng, X.; Zeng, X.; Sun, R.; Ren, L. Adaptable Thermal Conductive, High Toughness and Compliant Poly(Dimethylsiloxane) Elastomer Composites Based on Interfacial Coordination Bonds. *Compos. Sci. Technol.* **2023**, *231*, No. 109840.

(47) Ma, Z.; Zhao, B.; Gao, H.; Gong, Y.; Yu, R.; Tan, Z. Recent Advances of Crosslinkable Organic Semiconductors in Achieving Solution-Processed and Stable Optoelectronic Devices. *J. Mater. Chem. A* **2022**, *10* (36), 18542−18576.

(48) Sun, H.; Guo, G.; Memon, S. A.; Xu, W.; Zhang, Q.; Zhu, J. H.; Xing, F. Recycling of Carbon Fibers from Carbon Fiber Reinforced Polymer Using Electrochemical Method. *Composites, Part A* **2015**, *78*, 10−17.

(49) Huang, Z.; Deng, Z.; Dong, C.; Fan, J.; Ren, Y. A Closed-Loop Recycling Process for Carbon Fiber Reinforced Vinyl Ester Resin Composite. *Chem. Eng. J.* **2022**, *446*, No. 137254.

(50) Lebedeva, E. A.; Astaf'eva, S. A.; Istomina, T. S.; Trukhinov, D. K.; Shamsutdinov, A. S.; Strel'nikov, V. N.; Kukharenko, A. I.; Zhidkov, I. S. Novel Approach to Recycled Carbon Fiber Suitability Assessment for Additive Technologies. *Appl. Surf. Sci.* **2022**, *602*, No. 154251.

(51) Sun, W.; Luo, Y.; Sun, H. Experimental Studies on the Elastic Properties of Carbon Fiber Reinforced Polymer Composites Prefabricated of Unidirectional Carbon Fiber Fabrics and a Modified Rule of Mixtures in the Parallel Direction. *Adv. Compos. Lett.* **2018**, *27* (1), 34−43.

(52) Sayam, A.; Rahman, A. N. M. M.; Rahman, M. S.; Smriti, S. A.; Ahmed, F.; Rabbi, M. F.; Hossain, M.; Faruque, M. O. A Review on Carbon Fiber-Reinforced Hierarchical Composites: Mechanical Performance, Manufacturing Process, Structural Applications and Allied Challenges. *Carbon Lett.* **2022**, *32* (5), 1173−1205.

(53) Yanai, T.; Tew, D. P.; Handy, N. C. A New Hybrid Exchange−Correlation Functional Using the Coulomb-Attenuating Method (CAM-B3LYP). *Chem. Phys. Lett.* **2004**, *393* (1−3), 51−57.

(54) Neese, F. Software Update: The ORCA Program System—Version 5.0. *Wiley Interdisc. Rev.: Comput. Mol. Sci.* **2022**, *12* (5), No. e1606.